Hierarchical Free-Standing Carbon-Nanotube Paper Electrodes with Ultrahigh Sulfur-Loading for Lithium–Sulfur Batteries

Zhe Yuan, Hong-Jie Peng, Jia-Qi Huang, Xin-Yan Liu, Dai-Wei Wang, Xin-Bing Cheng, and Qiang Zhang**

The rational combination of conductive nanocarbon with sulfur leads to the formation of composite cathodes that can take full advantage of each building block; this is an effective way to construct cathode materials for lithium–sulfur (Li–S) batteries with high energy density. Generally, the areal sulfur-loading amount is less than 2.0 mg cm^{-2}, resulting in a low areal capacity far below the acceptable value for practical applications. In this contribution, a hierarchical free-standing carbon nanotube (CNT)-S paper electrode with an ultrahigh sulfur-loading of 6.3 mg cm^{-2} is fabricated using a facile bottom–up strategy. In the CNT–S paper electrode, short multi-walled CNTs are employed as the short-range electrical conductive framework for sulfur accommodation, while the super-long CNTs serve as both the long-range conductive network and the intercrossed mechanical scaffold. An initial discharge capacity of 6.2 mA·h cm^{-2} (995 mA·h g^{-1}), a 60% utilization of sulfur, and a slow cyclic fading rate of 0.20%/cycle within the initial 150 cycles at a low current density of 0.05 C are achieved. The areal capacity can be further increased to 15.1 mA·h cm^{-2} by stacking three CNT–S paper electrodes—resulting in an areal sulfur-loading of 17.3 mg cm^{-2}—for the cathode of a Li–S cell. The as-obtained free-standing paper electrode are of low cost and provide high energy density, making them promising for flexible electronic devices based on Li–S batteries.

1. Introduction

Electrical energy storage systems with superior performance are highly expected to address impending energy and environmental issues. Rechargeable lithium-ion (Li-ion) batteries are conventionally considered the most promising energy storage system due to their relatively high energy efficiency; however, they can no longer satisfy increasing demands for high energy density even though they almost reach the theoretical limit of electrode materials. Lithium–sulfur (Li–S) batteries have been seriously considered as an alternative as a result of their excellent theoretical energy density of 2567 W·h kg^{-1} (which is much higher than that of typical Li-ion batteries, e.g., 387 W·h kg^{-1} for a $LiCoO_2$/graphite system).[1] Although elemental sulfur is nontoxic and widely accessible at a low cost, the efficient use of sulfur as the cathode for rechargeable batteries is severely hindered by the insulating nature of sulfur-containing compounds and their complex multi-electron electrochemistry.

The flourishing fields of nanoscience and nanotechnology have resulted in advanced functional nanostructures for energy storage. When sulfur is combined with nanocarbons (e.g., carbon nanotubes (CNTs),[2,3] graphene,[4,5] macro-/meso-/microporous carbon,[6–8] carbon cloth,[9] carbon spheres,[10] and their hybrids[11,12]) or with conductive polymer nanostructures (e.g., polyaniline[13] and polypyrrole[14]), a composite cathode with good electrical conductivity and adequate free-space to accommodate volume expansion can be fabricated for the efficient use of sulfur. The nanostructured matrix with tunable surface properties retards the shuttle of soluble polysulfides between the cathode and anode, which improves the cycling performance.[15,16] To fully realize high-performance composite cathodes, the generally applied areal sulfur-loading on the electrode in previous investigations was generally less than 2.0 mg cm^{-2}.

In most reported Li–S cells, aluminum foil was employed as the current collector, and a routine slurry-coating procedure was used.[3–14] However, 10–50 wt% of the system comprised binders, conductive agents, and modifying precursors in the electrode, which neutralized the advantage of a Li–S system with high specific capacity. As the amount of areal sulfur-loading increased, the electrode film on the aluminum foil became thicker, and the transport efficiency for electrons and ions in the electrode decreased accordingly, which dramatically lowers the utilization ratio of sulfur. For instance, 77% and 36% utilization of sulfur, which correspond to 0.41 and 2.87 mA·h cm^{-2}

Z. Yuan,[+] H.-J Peng,[+] Dr. J.-Q. Huang, X.-Y. Liu, D.-W. Wang, X.-B. Cheng, Prof. Q. Zhang
Beijing Key Laboratory of Green Chemical Reaction Engineering and Technology
Department of Chemical Engineering
Tsinghua University
Beijing 100084, PR China
E-mail: jqhuang@tsinghua.edu.cn; zhang-qiang@mails.tsinghua.edu.cn
[+]Z. Yuan and H.-J. Peng contributed equally to this work.

DOI: 10.1002/adfm.201401501

and 1288 and 604 mA·h g_{sulfur}^{-1}, respectively, were achieved on electrodes fabricated by a routine slurry-coating method with areal sulfur-loadings of 0.32 and 4.77 mg cm^{-2}, respectively.[17] If the polymer binders and conductive agents can be replaced by highly conductive nanostructures, e.g., CNTs and graphene, 3D interlinked electron pathways and interconnected ion channels are available. For instance, both CNT[18] and graphene[4] can be used as the matrix to load 90 wt% of sulfur. Recently, an adhesive CNT film provided not only high electrical conductivity but also strong adhesive force, functioning simultaneously as both the conductive additive and the binder material for the Li-ion batteries.[19] In addition, CNTs can be further combined with other carbon–sulfur composites, e.g., (mesoporous carbon)–CNT–(sulfur composite microspheres) exhibiting a very high areal loading of 5 mg cm^{-2}, which offers a high reversible capacity of more than 700 mA·h g^{-1} after 200 cycles at a high current density of 2.8 mA cm^{-2} (0.56 A g^{-1}).[20] Solvent-free processing of the melt-infiltrated micro-/mesoporous carbide-derived carbon–sulfur nanocomposite, CNT conductive agent, and polytetrafluoroethylene binder was employed with an in-plane conductivity of up to 3 S cm^{-1} and an areal loading of 3.0 mg cm^{-2}.[21] A CNT–sulfur film with an areal loading of 5 mg cm^{-2} that was directly employed as the cathode in Li–S cells offers a reversible capacity of 740 mA·h g^{-1} after 100 charge/discharge cycles at 0.1 C (0.17 A g^{-1}).[22] A flexible cathode made from CNTs containing elemental sulfur at an areal loading of 2–3 mg cm^{-2}—which was synthesized by template-directed chemical vapor deposition, carbon thermo-reduction, and ethanol-evaporation-induced assembly—was reported to have a high discharge capacity of sulfur, 520 mA·h g^{-1}, on 50 wt% S at a high current density of 6.0 A g^{-1}.[23] Another free-standing sulfur electrode based on microporous carbon nanofibers and CNTs with a sulfur-loading of 0.8 mg cm^{-2} exhibited a reversible capacity of 637 mA·h g^{-1} after 100 cycles at 50 mA g^{-1} and a rate capability of 437 mA·h g^{-1} at 1 A g^{-1}.[24] Very recently, we found that using long CNTs as efficient conductive networks and using MgO-templated carbon nanocages as building blocks for sulfur accommodation with a high areal loading of 2.3 mg cm^{-2} resulted in electrodes with an initial discharge capacity of up to 1354 mA·h g^{-1} at 0.34 A g^{-1}.[25] The CNTs can serve as a high efficiency binder and conductive agent for the efficient use of sulfur; however, how to make full use of a hierarchical free-standing CNT electrode with both a high areal sulfur-loading capability and a high utilization efficiency of the active materials simultaneously remains a great challenge. The main considerations in the design of high-performance free-standing paper electrode are to assemble a CNT conductive scaffold and well-dispersed active materials for good electrical contact, a highly efficient electron pathway, interconnected ion channels, abundant space to accommodate a huge amount of active mass, and favorable mechanical durability.

In this contribution, we explore the fabrication of free-standing CNT–S paper electrodes by combining short- and long-range hierarchical CNT conductive networks, which are capable of ultrahigh sulfur-loading, ranging from 6.3 to 17.3 mg cm^{-2}. We selected short multi-walled CNTs (MWCNTs) with an average diameter of 15 nm and a length of 10–50 μm as the short-range electrical conductive network to support sulfur; we also used super-long CNTs with a diameter of 50 nm and a length of 1000–2000 μm from vertically aligned CNTs (VACNTs) as both the long-range conductive network and the inter-penetrating binders for the hierarchical free-standing paper electrode. In the bottom–up routine, sulfur was firstly well-dispersed into the MWCNT network to obtain MWCNT@S building blocks and then MWCNT@S and VACNTs were assembled into macro–CNT–S films via dispersion in ethanol followed by vacuum filtration (**Figure 1**). Note that no surfactant or additional surface modification to the CNTs was required because the adhesive sulfur on the CNTs weakened the strong interactions within the π-systems. These sulfur electrodes with hierarchical CNT scaffolds can accommodate more than 5–10 times the sulfur species that conventional electrodes on metal-foil current collectors can handle—while maintaining a high utilization of sulfur. Meanwhile, the sulfur-loading capability can be multiplied by the facile stacking of these electrodes into a layer-by-layer lasagna-like structure.

2. Results and Discussion

2.1. The Nanostructures of Hierarchical Free-Standing CNT Paper Electrodes

Our strategy involved the bottom–up synthesis of free-standing CNT–S paper electrodes with MWCNT@S and long VACNTs building blocks (Figure 1). First, the basic building blocks with MWCNT agglomerates and sulfur were fabricated via a melting–diffusion process; the sulfur was uniformly attached, and no bulky particles could be observed (Supporting Information (SI): Figure S1). The MWCNTs, which essentially comprise multilayered graphene rolled into a co-axial nanostructure with a *d*-spacing of 0.34 nm, exhibit high electrical conductivity along the *c*-axis, enabling them to provide efficient short-range electron pathways (**Figure 2**a). A thin sulfur layer uniformly coated the outer wall of the MWCNTs (Figure 2b).

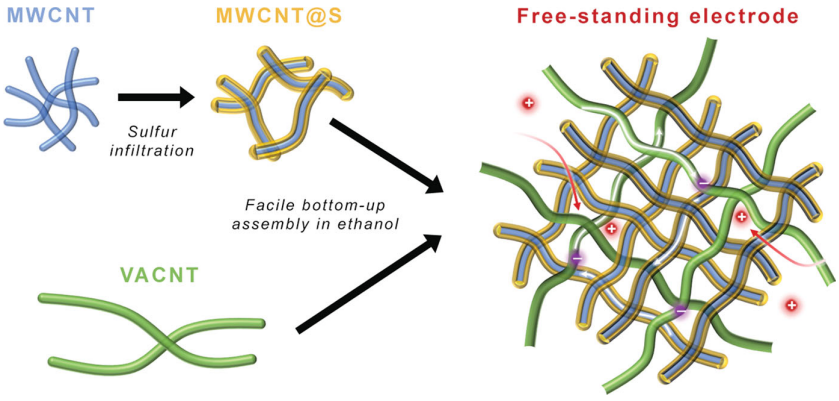

Figure 1. Schematic illustration of the hierarchical, free-standing electrode with ultrahigh sulfur-loading capability via a facile bottom–up approach. Red and purple spheres represent lithium ions and electrons, respectively.

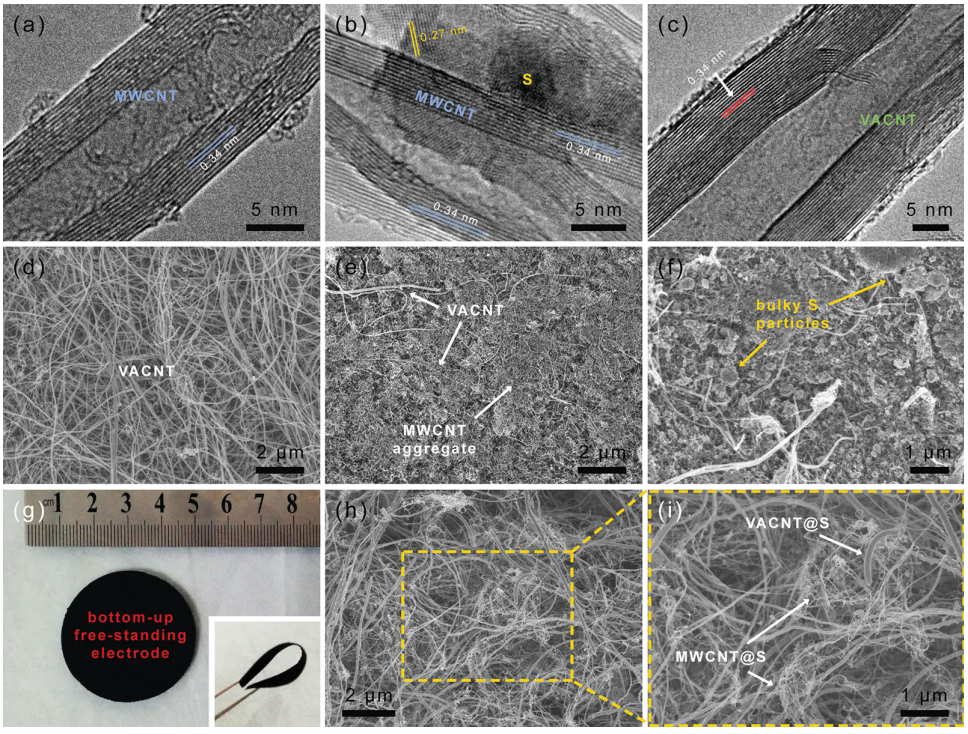

Figure 2. The morphology of CNT-based free-standing electrodes: a–c) Transmission electron microscopy (TEM) images of MWCNTs (a), MWCNT@S building blocks (b), and super-long VACNTs (c); d–f,h,i) Scanning electron microscopy (SEM) images of typical VACNT paper (d), VACNT/MWCNT paper (e), a top–down free-standing electrode produced by evaporation-induced precipitation of sulfur from toluene solution (f), and a bottom–up free-standing electrode (h) and the region surrounding the electrode in h (i). g) Photograph of the bottom–up free-standing electrode in both the extending and bending (inset) states.

An orthorhombic crystal pattern of sulfur was confirmed for the MWCNT@S sample, and a monoclinic phase was detected by X-ray diffraction for the CNT–S sample after co-heating at 155 °C (SI: Figure S2). The co-axial structure ensures good contact between the sulfur and carbon surface, which is beneficial to the short-range charge transfer. VACNTs with much larger diameter and length are more mechanically robust; they may serve as the long-range conducting agents, which essentially function as the structural skeleton of the paper electrode (Figure 2c). By changing the building blocks, VACNT paper, VACNT/MWCNT paper, and a bottom–up free-standing paper electrode composed of VACNTs and MWCNT@S were fabricated (Figure 2d–i and **Figure 3**).

VACNTs are easily assembled layer-by-layer into a robust film with a thickness of around 300 μm, in which each layer is around 5–10 μm thick (Figure 3a,d). The ultrahigh aspect ratio and good mechanical strength of VACNTs provide the paper electrode with a robust nanostructure. There is an abundance of 3D pores within the interconnected channels (Figure 2d). However, VACNTs cannot satisfy the demand for short-range electron transport because of their large diameters. A hierarchical electrode configuration in a VACNT/MWCNT paper was consequently proposed; this configuration could be fabricated using either a top–down or bottom–up process. Pristine MWCNTs tend to agglomerate due to strong van der Waals interactions even when vigorous shearing and high-aspect-ratio VACNTs are employed (Figure 2e). The VACNT/MWCNT paper, in which VACNTs were interwoven into the dense aggregates of the MWCNTs, was only 100 μm thick, but it had quite a high gravimetric density (Figure 3b,e). In order to serve as the cathode in a Li–S battery, sulfur was dissolved in toluene and added to the VACNT/MWCNT paper by toluene evaporation and sulfur precipitation. This top–down approach results in a free-standing electrode with poor distribution of the active sulfur in the conductive scaffolds. Bulky sulfur particles were attached to the CNT scaffolds due to the strong capillary force during solvent evaporation (Figure 2f). More importantly, the sulfur particles tended to deposit on the surface of the CNT paper instead of penetrating into the matrix; therefore, the interconnected channels for electrolyte penetration and ion diffusion were easily blocked.

In hopes of demonstrating the potential of CNT-based free-standing electrodes for energy storage applications, a bottom–up approach was also proposed. MWCNT@S building blocks with a good sulfur distribution and electrical contact between the CNT and sulfur were firstly fabricated. They were then dispersed into ethanol and then assembled with VACNTs. Large-area films exhibiting excellent flexibility without the help of any surfactants or binders could be produced (Figure 2g). Sulfur has a high affinity for the CNT surface via an interaction that is enhanced by π–π delocalization; these interactions weaken the strong packing and agglomerating tendency of CNTs. This is further confirmed by the increased thickness (~250 μm) and highly macroporous structure of the free-standing electrode produced with the bottom–up process in contrast to the VACNT/MWCNT papers (Figure 2h and 3c). In addition to the

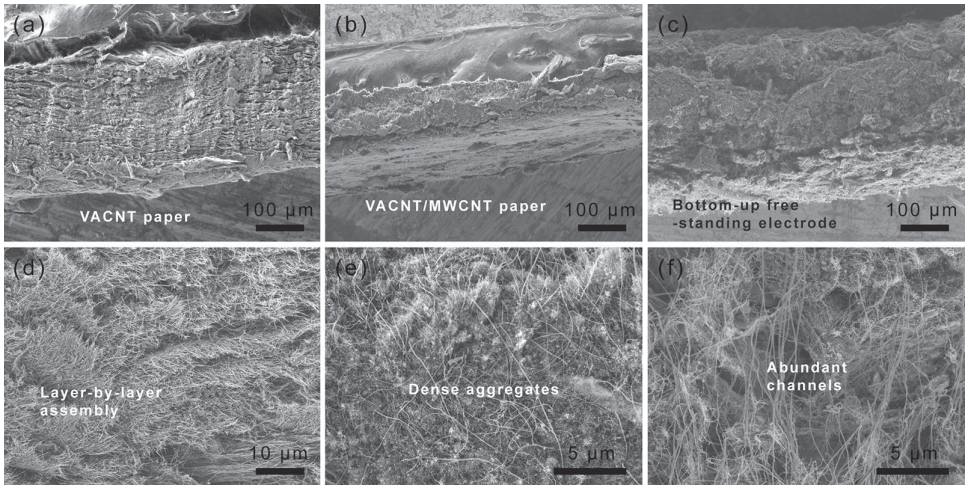

Figure 3. a–c) Low- and d–f) high-magnification SEM images of typical VACNT paper (a,d), VACNT/MWCNT paper (b,e), and bottom–up free-standing electrode (c,f).

VACNTs being highly dispersed forming a 3D macro-integrated skeleton, the MWCNT@S serve as expanded short-range networks instead of agglomerates (Figure 2i). Along the *c*-axis of the electrode, abundant channels constructed by intercrossed CNTs also favor the penetration of the electrolyte through the high-loading electrodes (Figure 3f). The electrical conductivity of the hierarchical electrode reached 17.1 S cm^{-1}, while using a similar sulfur-loading density and CNT additive amount, the electrode layer obtained from the routine slurry-coating process delivered an electrical conductivity of only 5.0 S cm^{-1}. The facile bottom–up approach results in good dispersion of the sulfur in the MWCNT matrix as well as among the VACNTs/MWCNTs in the whole electrode; consequently, highly efficient electron/ion pathways, fully utilized reactive interfaces, high sulfur-loading capability, and superior electrochemical properties are obtained. The areal sulfur-loading reached a very high value of 6.3 mg cm^{-2}, which is much higher than the previously reported electrode films produced using the routine slurry-coating method,[3–14] a CNT–S film,[22] or (mesoporous carbon)–CNT–sulfur composite microspheres.[20] Compared with aligned CNTs as the scaffolds,[2] herein the interlinked short- and long-range network provides intercrossed pores, which can be well preserved after a facile vacuum filtration procedure.

2.2. The Electrochemical Behavior of CNT Paper Electrodes

To explore the electrochemical behavior of the electrode with the ultrahigh sulfur-loading amount, a cyclic voltammetry (CV) test was conducted (**Figure 4**a). Although the areal sulfur-loading reached 6.3 mg cm^{-2}, the reduction peaks at the cathodic scans of 2.27 and 1.95 V present a typical two-step reduction of sulfur into high-order polysulfide and Li_2S/Li_2S_2, respectively. While in the anodic scan, the oxidation peaks at 2.34 and 2.45 V correspond to the transformation of Li_2S into high-order polysulfide and eventually to elemental sulfur, respectively. Compared with CV profiles obtained for samples involving a slurry-coating process on an aluminum current collector with an areal sulfur-loading of 0.4–2.0 mg cm^{-2},[11,26] both the cathodic and anodic peaks were obviously broadened due to the slower dynamics induced by the high loading amount of sulfur and increased thickness of the electrode. It should be noted that the several CV curves overlapped well, suggesting robust electrochemical reversibility in the free-standing paper electrodes.

Figure 4b presents the cyclic performance of the electrode at a current density of 0.05 C (0.38 mA cm^{-2}). The initial discharge capacity of the bottom–up free-standing electrode reaches 995 mA·h g^{-1}, which is 60% of the theoretical value for elemental sulfur. Meanwhile, the cyclic fading rate is as low as 0.20%/cycle. A discharge capacity of around 700 mA·h g^{-1} can be preserved within 150 cycles corresponding to a cycling lifespan of over 4 months. In comparison, the top–down paper electrode delivers a lower initial discharge capacity of 641 mA·h g^{-1}, which is attributed to the low utilization of the bulk sulfur particles. Furthermore, the capacity of the top–down free-standing electrode remains only less than 20 cycles and then rapidly degrades to less than 200 mA·h g^{-1} in 80 cycles. This is ascribed to the large volume of sulfur aggregates and its lithiated products blocking the ion channels and decreasing the accessibility to the active materials. The electrode fabricated using the routine slurry-coating process with a similar sulfur content also affords a limited initial capacity of 548 mA·h g^{-1}, and a higher capacity fading rate of 0.52%/cycle in 120 cycles.[17] The comparison indicates the superiority of the nanostructures fabricated using the bottom–up process, which results in all the components being well-dispersed, enabling demonstration of their roles as active materials, conductive scaffolds, and intermediate reservoirs. During charge–discharge cycling, the intermediate polysulfides are dissolved into the electrolyte. Due to their spontaneous redox reaction and free diffusion in the electrolyte between the anode and cathode, the polysulfides induce a shuttle phenomenon that induces a low capacity and poor cycling performance. The intrinsic diffusion of polysulfides in the liquid electrolyte among the porous nanocarbon framework renders a strong influence on the efficient utilization of sulfur in the cathode. The hierarchical electrode proposed herein via the bottom–up strategy with a sufficient thickness and an abundance of pores in the structure

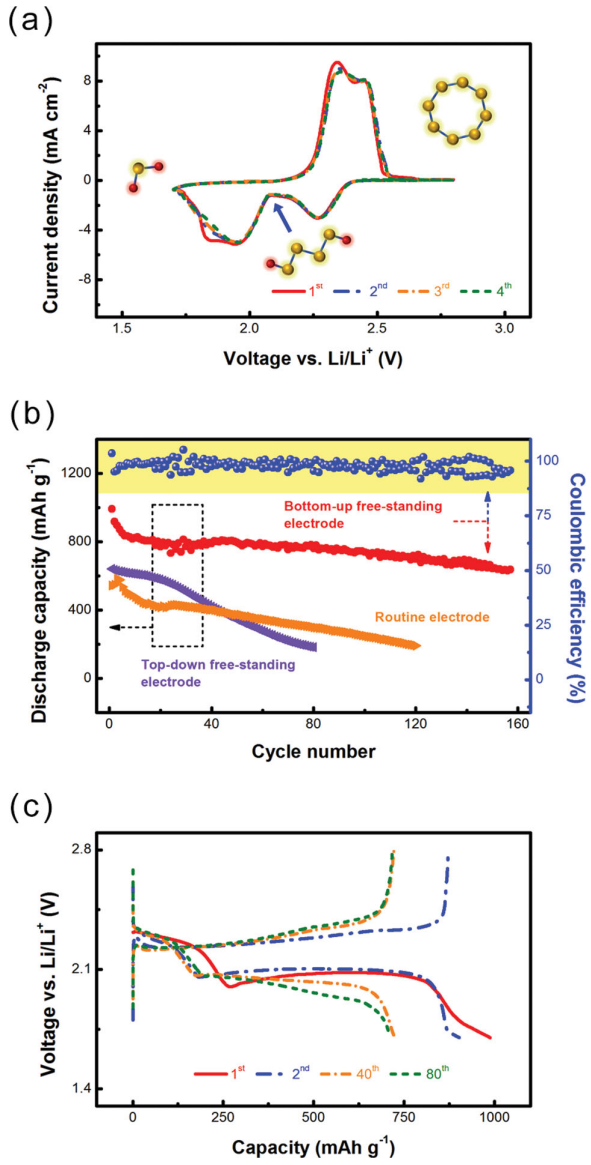

Figure 4. The electrochemical behavior of the bottom–up free-standing electrodes with ultrahigh sulfur-loading: a) CV profiles with insets showing the corresponding S species; yellow and red spheres represents S and Li atoms, respectively; b) cycling performance at a current density of 0.05 C with the performance of the top–down free-standing electrode and of a routinely prepared electrode blade coated on an aluminum foil for comparison; and c) corresponding galvanostatic charge–discharge curves of bottom-up free-standing electrodes at different cycles.

may effectively trap the polysulfides in the electrode matrix and suppress the shuttle effect. Synergistically with lithium nitrate ($LiNO_3$) additives,[27] the mean Coulombic efficiency reaches 97.9%. Several other strategies have been proposed to retard the shuttle of polysulfides via electrolyte modification. For instance, the incorporation of porous polysulfide reservoirs[28] or polymer chains (such as polyvinylpyrrolidone[29] and polyethylene glycol[6,26,30,31]) as well as the use of electrolyte with a highly concentrated lithium salt[8,32] or solvent-in-salt electrolyte,[33] and $LiNO_3$[27] containing electrolyte effectively suppressed the redox shuttle of the dissolved lithium polysulfides. Additionally, the use of a cation-permselective membrane resulted in electrostatic interactions and subsequently allowed lithium ions to diffuse across the membrane.[34] The addition of a nanocarbon (e.g., graphene[35] or CNT[36]) paper as a pseudo-upper current collector can also localize and retain the dissolved active material during cycling. The rational combination of these concepts with a high-loading CNT–S paper cathode is expected to further suppress the shuttle effect and greatly improve the cycling stability of the Li–S cells.

According to the voltage profiles of the bottom–up electrode (Figure 4c), the main discharge plateau corresponding to the transformation to Li_2S occurred during the first cycle at 2.10 V and decreased to 1.95 V in the 80th cycle. Although the electrode has a thickness of over 250 μm and an ultrahigh sulfur-loading of 6.3 mg cm^{-2}, the polarization during the electrochemical cycles remains at an acceptable level, which may also contribute to the highly efficient charge and ion transfer pathways. Furthermore, the highly porous 3D structure is also effective in trapping polysulfides, as indicated by the constant high plateaus corresponding to the generation of high-order polysulfides.

The rate performance of the CNT paper electrode is illustrated in the SI (Figure S3). The discharge capacities of 1093, 905, and 814 mA·h g^{-1} were achieved at a current density of 0.38, 0.76, and 1.51 mA cm^{-2}, respectively. A capacity retention of 74.5% was determined as the current increased from 0.38 to 1.51 mA cm^{-2}, which is competitive with other paper electrode reported in the literature.[19–24] The Li-ion diffusion length became larger as the electrodes increased thickness; therefore, the discharge capacity retention is not as competitive with very thin or porous electrodes.

2.3. Ultrahigh Areal Capacity of CNT Electrodes with Layer-by-Layer Lasagna-Like Structure

The interlinked structure without a metal foil as the current collector also endows this bottom–up free-standing paper electrode with the capability to reach even higher areal capacity in cell assembly. The areal capacity of the cathode materials is commonly around 4.0 mA·h cm^{-2} for commercially available lithium-ion batteries.[16] The majority of the research focused on Li–S batteries indicates that the areal capacity of the sulfur cathode is normally less than 1.0 mA·h cm^{-2};[26,30] this is far below the value that can be accepted by industry. In this work, the interlinked long CNTs, which function as a nanostructured binder and long-range collector, make it possible to multiply the sulfur-loading amount in the cells by simply stacking the paper electrodes in a layer-by-layer lasagna-like structure. The multistep discharge behavior is maintained with low polarization while the initial capacity is increased as the number of electrode layers increases (**Figure 5**a). This is attributed to the fact that 1) the highly porous 3D nanostructure provides abundant interconnected channels for electrolyte penetration even though the thickness of the integrated electrode is tripled and 2) the relative dead volume of the cell to the mass of sulfur is lowered, retarding irreversible loss of active materials and improving the initial utilization. Thus, the areal capacity of the cathode materials reaches 6.2 mA·h cm^{-2} with

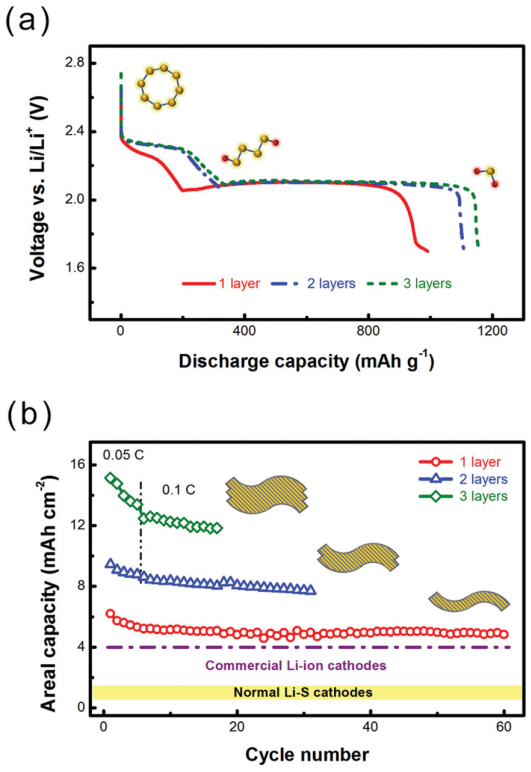

Figure 5. High areal capacities of stacked lasagna-like structured electrodes: a) galvanostatic discharge curves (with Li and S species indicated as insets; yellow and red spheres represent S and Li atoms, respectively; and b) cycling performance (with insets depicting the corresponding electrode structures).

a single electrode and exhibits good cycling stability. Even after 60 cycles, the areal capacity of the paper electrode is still higher than the current criteria for Li-ion batteries, which is 4.0 mA·h cm^{-2} (Figure 5b). The areal capacity of a single-layer paper electrode is much higher than that of the (micro-sized spherical carbon)–CNT–sulfur composite cathode with a sulfur-loading amount of 5.0 mg cm^{-2} (3.5 mA·h cm^{-2} after 200 cycles at a high current density of 2.8 mA cm^{-2}),[20] that of the CNT–sulfur electrode with a sulfur-loading of 5.0 mg cm^{-2} (3.7 mA·h cm^{-2} after 100 charge/discharge cycles at 0.1 C), and that of the CNT–(carbon nanocage)–sulfur electrode with an areal loading of 2.3 mg cm^{-2} (3.1 mA·h cm^{-2} at 0.34 A g^{-1}).[22] In this contribution, using a double- and triple-layer cathode electrode with a loading of 10.9 and 17.3 mg cm^{-2} in the cell, respectively, the initial areal capacity can be significantly improved to 9.4 and 15.1 mA·h cm^{-2}, respectively. This unprecedented performance gives rise to not only possible practical applications of high-energy-density Li–S batteries, but also to the concept of a (bottom–up)-assembled CNT scaffold for advanced energy storage systems.

The bottom–up free-standing electrode comprising sulfur and short-/long-CNTs brings a series of advantages to electrode materials, including the following: 1) 3D hierarchical structure can accommodate ultrahigh amounts of active materials for high-energy-density electrodes with ultrahigh areal capacity. 2) The ultralong CNTs simultaneously set up a highly conductive and robust framework, ensuring highly efficient charge and ion transfer pathways. 3) With highly chemically stable CNTs as the framework, there is no need for a binder and metal current collector; the issues of the degradation of polymer binders and the corrosion of metal foils are thus avoided, and further improvements are possible in the energy density. 4) Highly porous scaffolds with large free-space serve as reservoir for intermediate polysulfides and accommodate discharge products with expanded volume (SI: Figure S4).

3. Conclusion

A free-standing CNT–S paper electrode with an ultrahigh sulfur-loading of 6.3 mg cm^{-2} was fabricated using a bottom–up strategy, in which short MWCNTs served as the short-range electrical conductive network and super-long CNTs acted as both the long-range conductive network and intercrossed binders. Compared with routine electrodes fabricated on aluminum-foil current collectors via the slurry-coating method, such CNT–S paper electrodes accommodated over 5–10 times sulfur. An initial discharge capacity of 6.2 mA·h cm^{-2} (995 mA·h g^{-1}), a 60% utilization of sulfur, and a slow cyclic fading rate of 0.20%/cycle within the initial 150 cycles at a low current density of 0.05 C were achieved. The areal capacity of the CNT–S paper electrode is much higher than the value of 4.0 mA·h cm^{-2} for commercial Li-ion batteries. The areal capacity can be increased to 15.1 mA·h cm^{-2} by facile stacking of three CNT–S paper electrodes with an areal sulfur-loading of 17.3 mg cm^{-2} as the cathode in a Li–S cell. This proof-of-concept experiment indicates that the rational design of the nanostructured electrode offers the possibility to efficiently use the active materials at practical loading. The current bottom–up electrode fabrication procedure is effective for the preparation of large-scale flexible paper electrodes with a good distribution of all functional compounds; this procedure is also potentially applicable to graphene, CNT–graphene, and CNT–(metal oxide)-based flexible electrodes. The as-obtained free-standing paper electrode is promising for the ubiquitous application of Li–S batteries at a low cost and at high energy densities for future flexible electronic devices, such as smart electronics and roll-up displays.

4. Experimental Section

Raw Materials: The MWCNTs employed in this contribution were fabricated via a fluidization process on a Fe-based catalyst.[37] The very long VACNTs were synthesized by an improved floating catalyst method, as previously reported.[38] A routine purification procedure, in which the raw carbon products were purified using 12.0 M NaOH at 160 °C for 4.0 h and subsequently using 5.0 M HCl at 70 °C for another 4.0 h, was carried out. The sulfur powder with a high purity of >99.9% was purchased from Alfa Aesar and used without further purification.

Free-Standing Electrode Fabrication: The building blocks in the free-standing paper electrode were MWCNTs, long CNTs dispersed from VACNTs, and a sulfur phase. During the bottom–up fabrication, the MWCNTs were first mixed with sulfur; then the MWCNT@S building blocks were self-organized into the long CNT scaffolds. More precisely, 15.0 g of MWCNTs and 35.0 g of sulfur were mixed by milling in a mortar. The as-obtained mixture was then co-heated at 155 °C in a sealed flask for 2 h, and it was continued to be maintained under vacuum at the same temperature for another 0.5 h. Some of the sulfur

sublimed; therefore, a weight ratio of 63 wt% sulfur was determined in the MWCNT@S building blocks. The MWCNT@S powder (90 mg) and VACNTs (15 mg) were introduced into 120 mL of ethanol saturated with sulfur. A FLOKU high-shear emulsifier was used to disperse the above mentioned-mixture for 3.0 min. The CNT–S flexible paper electrode was fabricated via facile vacuum filtration. The as-obtained flexible paper electrode with a sulfur ratio of 54 wt% could be easily peeled off from the microporous filtering film after thorough drying at 60 °C for 24 h. The other procedure for a free-standing electrode was the top–down fabrication, in which the MWCNT/VACNT paper electrode was fabricated by vacuum filtration at a mass ratio of 6:1; then sulfur penetrated into the paper as a toluene–sulfur solution was evaporated at 70 °C. The free-standing electrode was punched into smaller disks with a diameter of 13 mm, which directly served as the working cathodes. Another control electrode fabricated using the routine slurry-coating method was also produced for this contribution. Typically, the cathode slurry was first prepared by mixing 85% of the MWCNT@S powder and 15% of the poly(vinylidene fluoride) binder in a *N*-methyl-2-pyrrolidone solvent dispersant. Then the slurry was coated onto aluminum foils using a doctor-blade, dried at 60 °C for 24 h, and punched into disks for the Li-ion storage performance evaluation.

Structural Characterization: The morphology of the paper electrodes was characterized by a JSM 7401F (JEOL Ltd., Tokyo, Japan) SEM operated at 3.0 kV and a JEM 2010 (JEOL Ltd, Tokyo, Japan) TEM operated at 120.0 kV. The structure of the sulfur in the electrode was determined by an X-ray powder diffractometer (D8-Advance, Bruker, Germany).

Electrochemical Evaluation: The standard 2025 coin-type cell was employed for electrochemical measurements. Lithium foil was used as the counter-electrode, and Celgard 2400 polypropylene membranes acted as separators. The electrolyte was 1 M lithium bis(trifluoromethanesulfonyl)imide and 0.25 M $LiNO_3$ dissolved in mixed solution of 1,3-dioxolane and 1,2-dimethoxyethane (v/v = 1/1) as solvent. Electrolyte aliquots of 80, 120, and 160 µL were added to the cells with one, two, and three layers of the paper electrode disks, respectively. The coin cells were tested in galvanostatic mode within a voltage range of 1.7–2.8 V using a Neware multichannel battery cycler. The CV measurements were performed on a Solartron 1470E electrochemical workstation at a scan rate of 0.1 mV s^{-1}. The gravimetric capacitance was calculated based on the mass of sulfur in the cathode, and the areal capacitance was derived based on the area of the electrode in a Li–S cell.

Supporting Information

Supporting Information is available from the Wiley Online Library or from the author.

Acknowledgements

This work was supported by the the National Natural Science Foundation of China (21306103), the China Postdoctoral Science Foundation (2012M520293, 2013T60125), and the Research Fund for the Doctoral Program of Higher Education of China (20120002120047).

Received: May 8, 2014
Revised: June 21, 2014
Published online: July 31, 2014

[1] a) D. W. Wang, Q. C. Zeng, G. M. Zhou, L. C. Yin, F. Li, H. M. Cheng, I. R. Gentle, G. Q. M. Lu, *J. Mater. Chem. A* **2013**, *1*, 9382; b) Y. Yang, G. Y. Zheng, Y. Cui, *Chem. Soc. Rev.* **2013**, *42*, 3018; c) H. Gwon, J. Hong, H. Kim, D. H. Seo, S. Jeon, K. Kang, *Energy Environ. Sci.* **2014**, *7*, 538.

[2] M. Hagen, S. Dorfler, P. Fanz, T. Berger, R. Speck, J. Tubke, H. Althues, M. J. Hoffmann, C. Scherr, S. Kaskel, *J. Power Sources* **2013**, *224*, 260.

[3] a) L. N. Wang, Y. Zhao, M. L. Thomas, H. R. Byon, *Adv. Funct. Mater.* **2014**, *24*, 2248; b) H. J. Peng, T. Z. Hou, Q. Zhang, J. Q. Huang, X. B. Cheng, M. Q. Guo, Z. Yuan, L. Y. He, F. Wei, *Adv. Mater. Interfaces* **2014**, *1*, 1400227; c) Y. Z. Fu, Y. S. Su, A. Manthiram, *Angew. Chem. Int. Ed.* **2013**, *52*, 6930.

[4] S. Evers, L. F. Nazar, *Chem. Commun.* **2012**, *48*, 1233.

[5] a) C. X. Zu, A. Manthiram, *Adv. Energy Mater.* **2013**, *3*, 1008; b) M.-Q. Zhao, Q. Zhang, J.-Q. Huang, G.-L. Tian, J.-Q. Nie, H.-J. Peng, F. Wei, *Nat. Commun.* **2014**, *5*, 3410; c) G. M. Zhou, L. C. Yin, D. W. Wang, L. Li, S. F. Pei, I. R. Gentle, F. Li, H. M. Cheng, *ACS Nano* **2013**, *7*, 5367; d) C. Zhang, W. Lv, W. Zhang, X. Zheng, M.-B. Wu, W. Wei, Y. Tao, Z. Li, Q.-H. Yang, *Adv. Energy Mater.* **2014**, *4*, 1301565; e) W. Lv, Z. Li, G. Zhou, J.-J. Shao, D. Kong, X. Zheng, B. Li, F. Li, F. Kang, Q.-H. Yang, *Adv. Funct. Mater.* **2014**, *24*, 3456; f) X. Yang, L. Zhang, F. Zhang, Y. Huang, Y. S. Chen, *ACS Nano* **2014**, *8*, 5208.

[6] X. L. Ji, K. T. Lee, L. F. Nazar, *Nat. Mater.* **2009**, *8*, 500.

[7] L. Yu, N. Brun, K. Sakaushi, J. Eckert, M. M. Titirici, *Carbon* **2013**, *61*, 245.

[8] J. T. Lee, Y. Zhao, S. Thieme, H. Kim, M. Oschatz, L. Borchardt, A. Magasinski, W. I. Cho, S. Kaskel, G. Yushin, *Adv. Mater.* **2013**, *25*, 4573.

[9] X. G. Han, Y. H. Xu, X. Y. Chen, Y. C. Chen, N. Weadock, J. Y. Wan, H. L. Zhu, Y. L. Liu, H. Q. Li, G. Rubloff, C. S. Wang, L. B. Hu, *Nano Energy* **2013**, *2*, 1197.

[10] a) N. Jayaprakash, J. Shen, S. S. Moganty, A. Corona, L. A. Archer, *Angew. Chem. Int. Ed.* **2011**, *50*, 5904; b) F. Bottger-Hiller, P. Kempe, G. Cox, A. Panchenko, N. Janssen, A. Petzold, T. Thurn-Albrecht, L. Borchardt, M. Rose, S. Kaskel, C. Georgi, H. Lang, S. Spange, *Angew. Chem. Int. Ed.* **2013**, *52*, 6088; c) G. He, S. Evers, X. Liang, M. Cuisinier, A. Garsuch, L. F. Nazar, *ACS Nano* **2013**, *7*, 10920; d) J. Liu, T. Y. Yang, D. W. Wang, G. Q. M. Lu, D. Y. Zhao, S. Z. Qiao, *Nat. Commun.* **2013**, *4*, 2798.

[11] M. Q. Zhao, X. F. Liu, Q. Zhang, G. L. Tian, J. Q. Huang, W. C. Zhu, F. Wei, *ACS Nano* **2012**, *6*, 10759.

[12] a) S. Xin, L. Gu, N. H. Zhao, Y. X. Yin, L. J. Zhou, Y. G. Guo, L. J. Wan, *J. Am. Chem. Soc.* **2012**, *134*, 18510; b) X. Y. Zhou, J. Xie, J. Yang, Y. L. Zou, J. J. Tang, S. C. Wang, L. L. Ma, Q. C. Liao, *J. Power Sources* **2013**, *243*, 993; c) X. A. Chen, Z. Xiao, X. Ning, Z. Liu, Z. Yang, C. Zou, S. Wang, X. Chen, Y. Chen, S. Huang, *Adv. Energy Mater.* **2014**, *4*, 1301988; d) C. Tang, Q. Zhang, M.-Q. Zhao, J.-Q. Huang, X.-B. Cheng, G.-L. Tian, H.-J. Peng, F. Wei, *Adv. Mater.* **2014**, DOI: 10.1002/adma.201401243; e) H.-J. Peng, J.-Q. Huang, M.-Q. Zhao, Q. Zhang, X.-B. Cheng, X.-Y. Liu, W.-Z. Qian, F. Wei, *Adv. Funct. Mater.* **2014**, *24*, 2772.

[13] J. L. Wang, J. Yang, J. Y. Xie, N. X. Xu, *Adv. Mater.* **2002**, *14*, 963.

[14] Y. Z. Fu, A. Manthiram, *J. Phys. Chem. C* **2012**, *116*, 8910.

[15] a) L. W. Ji, M. M. Rao, H. M. Zheng, L. Zhang, Y. C. Li, W. H. Duan, J. H. Guo, E. J. Cairns, Y. G. Zhang, *J. Am. Chem. Soc.* **2011**, *133*, 18522; b) Z. Liang, G. Y. Zheng, W. Y. Li, Z. W. Seh, H. B. Yao, K. Yan, D. S. Kong, Y. Cui, *ACS Nano* **2014**, *8*, 5249.

[16] J. X. Song, T. Xu, M. L. Gordin, P. Y. Zhu, D. P. Lv, Y. B. Jiang, Y. S. Chen, Y. H. Duan, D. H. Wang, *Adv. Funct. Mater.* **2014**, *24*, 1243.

[17] L. Zhu, W. Zhu, X.-B. Cheng, J.-Q. Huang, H.-J. Peng, S.-H. Yang, Q. Zhang, *Carbon* **2014**, *75*, 161.

[18] X. B. Cheng, J. Q. Huang, Q. Zhang, H. J. Peng, M. Q. Zhao, F. Wei, *Nano Energy* **2014**, *4*, 65.

[19] Z. Y. Cao, B. Q. Wei, *ACS Nano* **2014**, *8*, 3049.

[20] T. Xu, J. X. Song, M. L. Gordin, H. Sohn, Z. X. Yu, S. R. Chen, D. H. Wang, *ACS Appl. Mater. Interfaces* **2013**, *5*, 11355.

[21] S. Thieme, J. Bruckner, I. Bauer, M. Oschatz, L. Borchardt, H. Althues, S. Kaskel, *J. Mater. Chem. A* **2013**, *1*, 9225.

[22] K. K. Jin, X. F. Zhou, L. Z. Zhang, X. Xin, G. H. Wan, Z. P. Liu, *J. Phys. Chem. C* **2013**, *117*, 21112.
[23] G. M. Zhou, D. W. Wang, F. Li, P. X. Hou, L. C. Yin, C. Liu, G. Q. Lu, I. R. Gentle, H. M. Cheng, *Energy Environ. Sci.* **2012**, *5*, 8901.
[24] L. C. Zeng, F. S. Pan, W. H. Li, Y. Jiang, X. W. Zhong, Y. Yu, *Nanoscale* **2014**, DOI: 10.1039/C4NR02498B.
[25] J. Q. Huang, H. J. Peng, X. Y. Liu, J. Q. Nie, X. B. Cheng, Q. Zhang, F. Wei, *J. Mater. Chem. A* **2014**, *2*, 10869.
[26] S. M. Zhang, Q. Zhang, J. Q. Huang, X. F. Liu, W. C. Zhu, M. Q. Zhao, W. Z. Qian, F. Wei, *Part. Part. Syst. Char.* **2013**, *30*, 158.
[27] D. Aurbach, E. Pollak, R. Elazari, G. Salitra, C. S. Kelley, J. Affinito, *J. Electrochem. Soc.* **2009**, *156*, A694.
[28] a) X. L. Ji, S. Evers, R. Black, L. F. Nazar, *Nat. Commun.* **2011**, *2*, 325; b) K. H. Kim, Y.-S. Jun, J. A. Gerbec, K. A. See, G. D. Stucky, H.-T. Jung, *Carbon* **2014**, *69*, 543; c) M.-S. Park, B. O. Jeong, T. J. Kim, S. Kim, K. J. Kim, J.-S. Yu, Y. Jung, Y.-J. Kim, *Carbon* **2014**, *68*, 265.
[29] G. Y. Zheng, Q. F. Zhang, J. J. Cha, Y. Yang, W. Y. Li, Z. W. Seh, Y. Cui, *Nano Lett.* **2013**, *13*, 1265.
[30] J. Q. Huang, X. F. Liu, Q. Zhang, C. M. Chen, M. Q. Zhao, S. M. Zhang, W. C. Zhu, W. Z. Qian, F. Wei, *Nano Energy* **2013**, *2*, 314.
[31] a) H. Wang, Y. Yang, Y. Liang, J. T. Robinson, Y. Li, A. Jackson, Y. Cui, H. Dai, *Nano Lett.* **2011**, *11*, 2644; b) J. Q. Huang, Q. Zhang, S. M. Zhang, X. F. Liu, W. C. Zhu, W. Z. Qian, F. Wei, *Carbon* **2013**, *58*, 99.
[32] E. S. Shin, K. Kim, S. H. Oh, W. I. Cho, *Chem. Commun.* **2013**, *49*, 2004.
[33] L. M. Suo, Y. S. Hu, H. Li, M. Armand, L. Q. Chen, *Nat. Commun.* **2013**, *4*, 1481.
[34] a) J. Q. Huang, Q. Zhang, H. J. Peng, X. Y. Liu, W. Z. Qian, F. Wei, *Energy Environ. Sci.* **2014**, *7*, 347; b) I. Bauer, S. Thieme, J. Bruckner, H. Althues, S. Kaskel, *J. Power Sources* **2014**, *251*, 417.
[35] G. M. Zhou, S. F. Pei, L. Li, D. W. Wang, S. G. Wang, K. Huang, L. C. Yin, F. Li, H. M. Cheng, *Adv. Mater.* **2014**, *26*, 625.
[36] Y. S. Su, A. Manthiram, *Chem. Commun.* **2012**, *48*, 8817.
[37] Q. Zhang, M.-Q. Zhao, D.-M. Tang, F. Li, J.-Q. Huang, B. Liu, W.-C. Zhu, Y.-H. Zhang, F. Wei, *Angew. Chem. Int. Ed.* **2010**, *49*, 3642.
[38] Q. Zhang, D. G. Wang, J. Q. Huang, W. P. Zhou, G. H. Luo, W. Z. Qian, F. Wei, *Carbon* **2010**, *48*, 2855.